Numerical Investigation of Topographical Site Effects: Parametric Study on Simplified Geometries and Impact of the Inner Geological Structure

N. Glinsky[(1)], E. Bertrand[(2)]

[(1)] *Research Scientist, CEREMA Dter Méd, Nice Laboratory and IFSTTAR Gers/SV, France, nathalie.glinsky@cerema.fr*
[(2)] *Research Scientist, CEREMA Dter Méd, Nice Laboratory, France, etienne.bertrand@cerema.fr*

Abstract

Amplification of the seismic ground motion is often observed in presence of strong topography or in sedimentary basins in which the seismic waves are trapped. The study of site effects can be achieved by the analysis of seismological recordings. Measurement campaigns at specific sites allowed highlighting high amplification for some frequencies but it is often difficult to deduce from the field data what are the main parameters responsible for local amplification. Numerical simulation is then an interesting tool for understanding such phenomena. In particular, it allows series of simulations in the frame of parametric studies.

In few decades, many numerical methods have been developed, improving their accuracy by including new numerical schemes and more complex physical models. They have been widely applied to lithological site effects, in sedimentary basins, but much less to study the topography influence. Many past studies which aimed at understanding these effects have been limited to homogeneous models and concluded that the numerical simulations underestimate the amplification levels of field data. Topography alone cannot produce the measured amplification levels; the medium in-depth must also be accurately described and heterogeneous models must be considered. This helps explaining the strong amplifications measured on very smooth hills.

The objective of this study is to use numerical simulations to improve the understanding of topographical site effects and, in particular, the influence of some parameters on the ground motion amplification at the surface. These simulations are done using a discontinuous Galerkin finite element method which is high-order accurate, flexible and allows an accurate description of the topography and the in-depth medium properties. This method is applied to the solution of the velocity-stress system in time domain to study the surface response to series of plane waves of various frequencies.

First, a very detailed parametric study is proposed for a canonical simplified geometry in order to exhibit the main parameters responsible for amplification. Then we consider a more realistic topography of the Rognes area, place where occurred the Provence earthquake (1909), the most significant French earthquake of the 20th century and compare the results of the simulations to the field measurements.

Keywords: site effects, topographical effects ,numerical simulation, discontinuous Galerkin, finite element method

1. Introduction

Ground motion estimation in inhabited areas is an essential step in seismic risk mitigation. Site effects, resulting from local geological and geotechnical conditions, require a particular attention. First reported by Singh et al. [1] during the 1985 Michoacan earthquake, site effects are generally observed in sedimentary basins or in presence of strong topography. Many studies, both experimental and numerical, have been conducted to explain amplification and increase in signal duration recorded at the surface of basins. Similar work was performed for topographical effects. Many parameters have been identified as responsible for strong amplifications but several observations are still not completely understood [2].

The effects of topography were highlighted through experimental studies based on recordings data. Massa et al. [2] propose a thorough review of some results of the literature which show that high values of the shape ratio or complex three-dimensional topographies lead to strong amplification. Yet, in some cases, contrary to what is expected, very strong motion is observed in gentle slopes or low hills as, for instance, in Tarzana [3,4], in Rognes [5] or in Haïti [6] which proves that these are very complex phenomena that cannot be justified by geometrical criteria. We aim to focus on such particular geometries.

The topography effects have also been investigated by numerical studies using idealized geometries. In few decades, many numerical methods were developed and have been naturally applied to this problem. Among the many contributions too numerous to detail here, we mention some pionnering studies, for instance, the seismic response of simplified 2D homogeneous topographies or slopes subject to SH and P-SV plane waves [7,8,9,10], the application to 3D homogeneous topographies [11] or the combination between effects of several topographies and near-surface layering [12,13]. These studies identified important parameters such as the shape ratio or the wavelength of the incident wave. Furthermore, the amplification is generally higher at the hill top with a high variability between the top and the hill foot. Numerical simulations have also been applied to realistic topographies and compared to measurements. As the knowledge about geological and geotechnical properties is limited, the medium is often supposed to be homogeneous which could be one of the reasons of the quantitative differences between measurements and simulations. Some recent studies [2,4,6] emphasize the importance of a detailed description of the in-depth medium for an accurate estimation of the ground motion. We will consider this aspect and compare homogeneous and heterogeneous models.

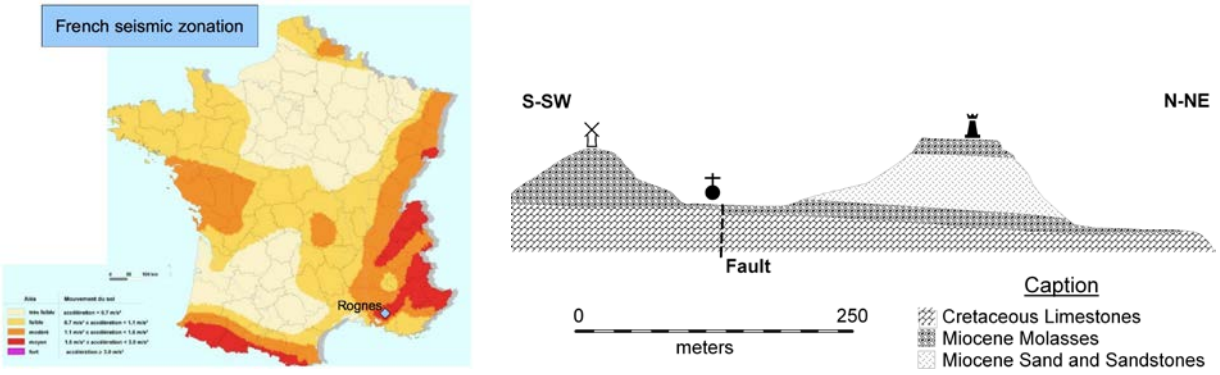

Fig. 1: French seismic zonation and location of the Rognes area (left). Simplified geological profile of the Rognes village (right).

The Provence earthquake (estimated Mw 6.0 [14]), which occurred in 1909 in the south of France, is the main French earthquake of the 20th century. It caused the death of more than 40 people and significant property damage. The village of Rognes, located approximately at 5km from the epicenter, was partly destroyed, especially the castle built on the small Foussa hill, probably due to site effects [5]. This area is located in the highest hazard zone of Metropolitan French seismic zonation, as illustrated in Fig.1 (left picture). The simplified geological profile of the area (Fig. 1, right) shows that the village is built between two small hills and provides a basis for a heterogeneous model to be used in simulations. To understand the damage during the Provence

earthquake and confirm the site effect in this particular location, the CEREMA Méditerranée Seismik Risk team conducted a two years field operation (2007-2009), achieving continuous recordings at nine selected sites (see Fig. 2 (left) for some of them). During the campaign, more than 70 earthquakes (10 local and 60 teleseismic events) were recorded and analyzed. Three results were deduced from these data: H/V ratios on ambient vibration, H/V ratios on earthquake and site/reference standard ratios (SSR) on earthquakes (Duval et al. [5]). We present, in Fig. 2 (right), the seismic response derived from near earthquakes recordings at three particular sites (EGLI, FOUS and, FOUH) as visible in Fig. 2. We note a strong amplification (between 4 and 7) at about 2Hz for two stations (FOUH and FOUS) located on the hill while a lower value of amplification, for a frequency greater than 5Hz, is obtained for a location at the hill foot (station EGLI).

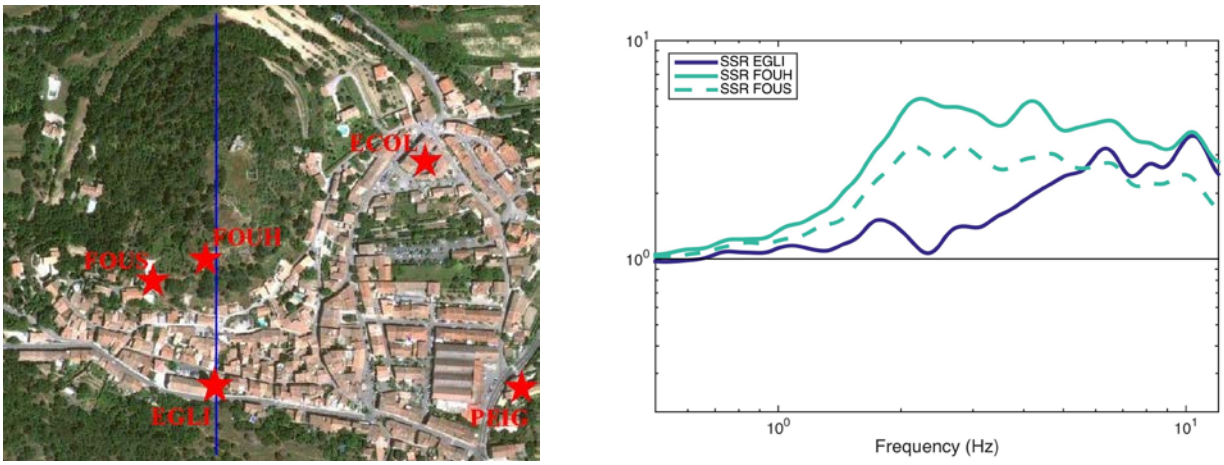

Fig. 2: Left: Aerial photography of the studied zone and location of some stations of the measurement campaign. The blue line corresponds to the south-north profile used for the numerical simulations. Right: Seismic response (SSR) at three stations (EGLI, FOUS and FOUH) from real measurements (near earthquakes).

The objective of this study is to propose numerical simulations of a realistic topography of Rognes area and try to understand and reproduce the results of the field measurements [2]. It constitutes an improvement of a first study proposed in [15] and focuses on the case of gentle slopes geometries as it is the case in Rognes. In a first part, we consider an idealized geometry and compare two configurations (homogeneous and heterogeneous), the effect of the frequency and the angle of the incident wave. In a second part, a similar study is proposed for a 2D profile of the Rognes model as well as comparisons with the measurement data.

2. Equations and numerical method

We consider the P-SV wave propagation in an isotropic and linearly elastic medium and solve the elastodynamic equations in velocity-stress formulation and time domain

$$\begin{cases} \rho \partial_t \vec{V} = \nabla \cdot \sigma, \\ \partial_t \sigma = \lambda \left(\nabla \cdot \vec{V} \right) I_d + \mu \left[\nabla \vec{V} + \left(\nabla \vec{V} \right)^t \right], \\ \sigma \vec{n} = \vec{0} \quad \text{on } \Gamma_{free\ surface}, \end{cases} \tag{1}$$

where the unknowns are the velocity vector $\vec{V}$ and the stress tensor σ. ρ, λ and μ are respectively the density of the medium and the Lamé parameters related to both shear and compressional velocities by

$$V_S = \sqrt{\frac{\mu}{\rho}} \quad \text{and} \quad V_P = \sqrt{\frac{\lambda + 2\mu}{\rho}}. \tag{2}$$

Id is the identity matrix and ∂_t refers to the time derivative. This system is approximated by a Galerkin discontinuous finite element method whose description and a detailed analysis can be found in [16,17]. Here, we only present the main characteristics of the method. The physical domain is discretized using a triangular finite element mesh. The interpolation of the unknowns is based on a second-degree Lagrange polynomials basis defined locally in each triangle which involves calculating numerical fluxes at the interfaces between triangles. The fluxes are estimated using a centered scheme. For time integration, we use a leap-frog scheme which leads to a method second-order accurate in time and space. On boundaries, except for the topography where a free surface condition is applied, we consider an upwind scheme which has two functions: first, it allows introducing an incident plane wave whatever the angle of incidence and secondly, it acts as an absorbing condition (when values coming from outside the numerical domain are set to zero).

3. Canonical case: application to an idealized hill topography

In a first step, we consider a simplified hill topography, as done in [18], whose surface equation is given by

$$s(x) = h(1-a)e^{-3a}, \qquad a = (x/l)^2, \tag{3}$$

where *h* and *l* are respectively the height and the half width of the hill. The surface topography is described in Fig. 3. Being interested in the case of a gentle slope, we set *h*/*l*=0.2 with *h*=500m. We consider two different configurations; a homogeneous medium, M1 of Table 1, and a heterogeneous model consisting in M1 at depth i.e. under the black line and M2 for the entire hill, as illustrated in Fig. 3. The heterogeneous model has been chosen because close to the geological model of Rognes, described in Fig. 1.

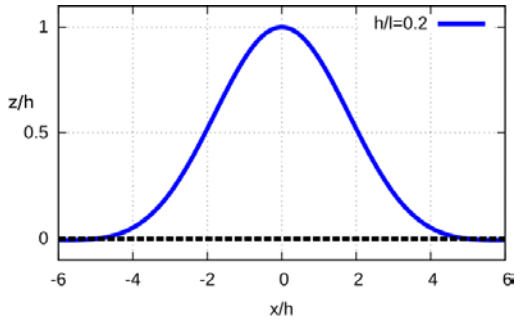

Fig.3: Simplified topography. For the homogeneous model, medium M1 and for the heterogeneous model, M1 at depth (under the black line) and M2 for the hill.

Table 1: Characteristics of the media of the homogeneous and heterogeneous canonical models.

	ρ(kg/m^3)	*Vp* (m/s)	*Vs*(m/s)
M1	2000	1870	1000
M2	1500	935	500

We study the response of this topography to series of plane shear waves. We construct two triangular unstructured meshes (for the homogeneous and heterogeneous models) using the free mesh generator Gmsh [19]. The computational domain is 12000m wide and 6000m deep and the topography is added at the center of the top surface. The mesh size is about 25m at the free surface and 50m in the bedrock and the two meshes contain approximately 153000 triangles. Free surface conditions are applied on the upper boundary of the domain and the upwind boundary flux for the three others. First, the source excitation is a vertically incident plane SV wave with a Ricker time dependence. The central frequency *fc* is chosen following two dimensionless parameters

frequently used in the literature, respectively based on the height $\eta h=h\ fc/Vs$ and the width of the hill $\eta l=2l\ fc/Vs$. For each parameter, we consider the three values $\eta_{h/l} \in \{0.5,1.0,2.0\}$, which corresponds to 6 simulations. Since h and l have fixed values, variations of ηl correspond to values for the central frequencies equal to 0.1, 0.2 and 0.4Hz whereas, for ηh, the values for fc are 1.0, 2.0 and 4.0Hz. For both models, the values of ηl and ηh are calculated from the velocity in the bedrock and the values of the frequency are the same. The correspondence between ηl, ηh and fc is given in Table 2.

Table 2: Correspondence between ηl, ηh and fc.

fc (Hz)	0.1	0.2	0.4	1.0	2.0	4.0
ηl	0.5	1.0	2.0	5.0	10.	20.
ηh	0.05	0.1	0.2	0.5	1.0	2.0

Solutions are recorded at 241 surface receivers uniformly distributed every 25m in the x interval [-3000;3000]. At each receiver, we calculate an amplification ratio A from time solutions defined as the ratio between the maximum of Vx recorded at the surface and twice the maximum of the same component of the incident wave (or equivalently the ratio between the Peak Ground Velocities). We present in Fig. 4, the distribution of the amplitude ratios at all surface receivers for the homogeneous (left) and the heterogeneous (right) models. Each picture contains the results of the 6 simulations corresponding to the various values for η or equivalently fc. As the solutions are symmetrical for vertical incidence, each figure is split in two parts, the left part corresponds to variations of ηl i.e. the lowest frequencies, and the right part to values of ηh. For clarity, the profile of the hill is reported in grey at the bottom of the figures and a thick line identifies amplifications values greater to 1.2 i.e. an increase in PGV greater than 20%.

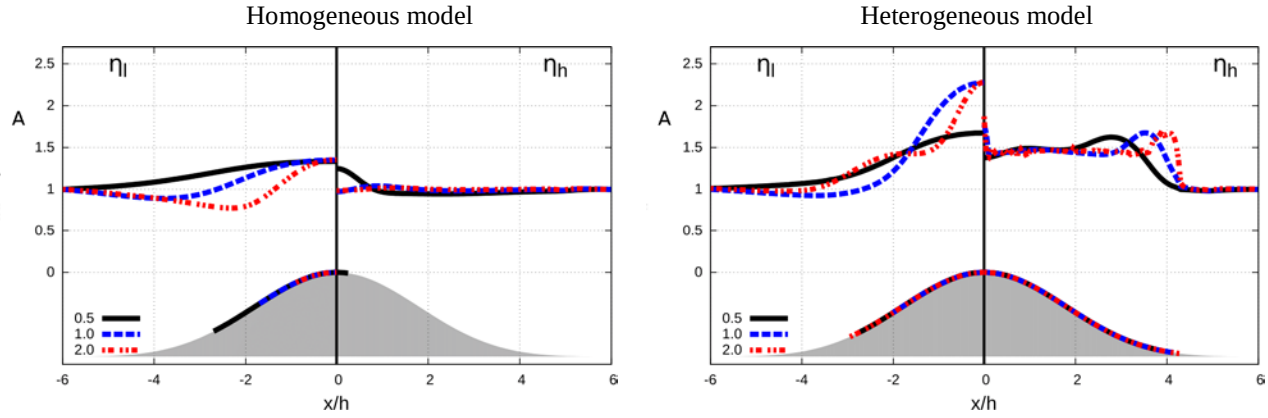

Fig.4: Amplification ratio A of Vx at the surface of the idealized topography, homogeneous model (left) and heterogeneous model (right). Incident plane wave, ηl=0.5, 1.0 and 2.0 for the left parts of both pictures and ηh=0.5, 1.0 and 2.0 for the right parts. The hill topography is included in grey at the bottom and lines at its surface correspond to amplifications greater than 20%.

In Fig. 4, we note that for the homogeneous model (left picture), the amplification is generally very low (less than 1.3) and occurs mostly at lower fc corresponding to the values of ηl (left half of the figure) for a wide part of the surface. A clear deamplification is observed on the flank for ηl=2.0 (dashed red line). For values of ηh (right half of the figure), there is no amplification for frequencies greater than 1.0Hz and for fc=0.5Hz, amplification is very localized at the hill top. When analyzing the heterogeneous case (right figure), we notice a significant increase in the amplification ratios which proves a strong influence of the in-depth model even for this case of gentle slopes. Amplification reaches values between 1.5 and 2.3 and all the surface of the hill is

concerned, especially for the highest values of the frequency. At the hill foot, where the low velocity medium becomes very thin, we notice a strong amplification. It depends on the particular geometry of our model. In this heterogeneous case, the waves are trapped in the hill and amplification as well as an increase in signal duration are observed.

We complete this study by considering the influence of the angle of incidence. In particular, the objective is to identify higher amplifications compared to the vertically incident case which could also explain the quantitative differences encountered between experimental and numerical studies. For this study, we consider the two same models (homogeneous and heterogeneous) but the angle of incidence a relative to the vertical varies between 0 and 25 degrees. As the hill geometry is symmetrical, we can restrict ourselves to positive values of the angle of incidence. We compare in Fig. 5 the results of the amplification ratios at the surface obtained for the homogeneous and heterogeneous models. We have plot on two separate figures the solutions corresponding to lower and higher values of the frequency but brought together solutions from various angles of incidence in order to have a global view. The different line types correspond to the frequency of the incident wave.

When comparing both results, we notice than for the homogeneous and heterogeneous models, the amplification levels are higher than for the vertical case and the amplification extends over a larger surface area. The maximum amplification is no more measured at the hill top. In the homogeneous case and lower values of frequency (top left figure), amplification is very low and limited to some cases. For higher frequencies (bottom left figure), the amplification depends more on the angle of incidence than on the frequency. Indeed, the highest amplifications correspond to various values of η. We also note than even if the angle of incidence is positive, amplification is not limited to one side of the topography whereas strong deamplifications occur only in the right part of the surface. In the heterogeneous case, the increase in the amplification level is extended to the whole topography surface and depends more on the frequency than on the angle of incidence, probably because the waves are trapped in the low velocity medium. For higher values of frequency (bottom right figure), all the topography surface is amplified but the maximum is mostly at or near the hill top.

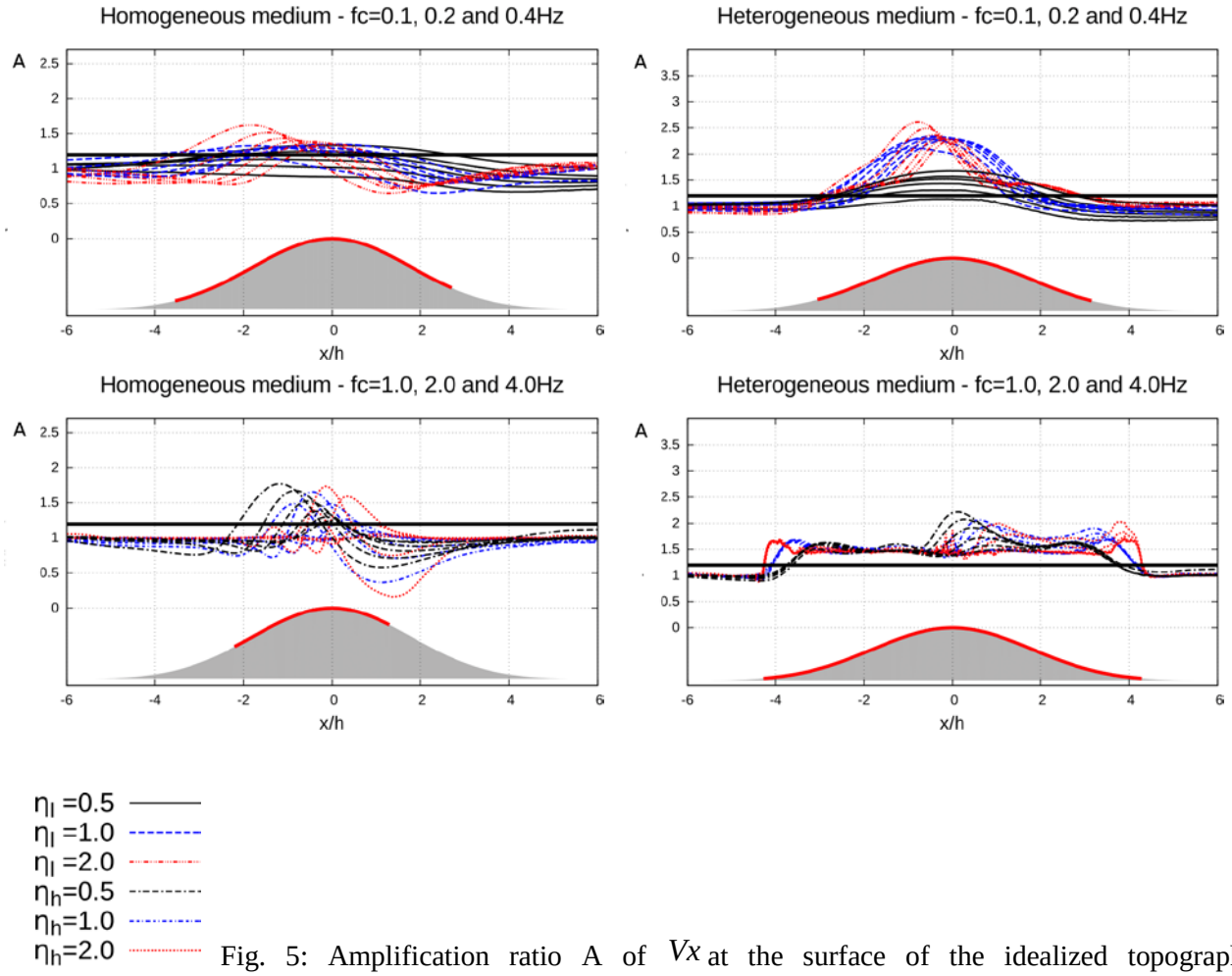

Fig. 5: Amplification ratio A of Vx at the surface of the idealized topography, homogeneous model (left) and heterogeneous model (right), various angles of incidence from 0 to 25 degrees. A line type corresponds to a value of ηl or ηh as mentioned above. The hill topography is included in grey at the bottom and lines at its surface correspond to amplifications greater than 20%. Note that vertical scales of the figures are different.

4. Application to a realistic profile of the Rognes area

In a second part, we consider a realistic 2D profile extracted from the topographic model of the Rognes area. This profile is a south-north line containing the top of the Foussa hill, represented by the blue line in Fig. 2 (left). The computational domain is 10km wide and 6km deep; the studied Rognes's topography represents the x interval [4000;5000] which is extended on both sides by flat parts. The upper boundary of the model is the topography (as shown in Fig.6) on which free surface conditions are applied; as previously, the upwind boundary flux is used for other boundaries. Two unstructured meshes are constructed using Gmsh. The mesh size is two times smaller than for the idealized topography for an accurate description of the surface; the meshes both contain approximately 372000 triangles. A detail of the mesh of the homogeneous model is shown in Fig. 6. Seven virtual sensors have been placed at different locations of the hill surface (as shown in Fig. 6). These locations have been chosen in accordance with the sites of the real data, shown in Fig. 2. For instance, the station 5 at the top of the hill of the 2D profile can be compared to the real station FOUH. Two models have been studied, a homogeneous model whose properties are those of medium M1 (see Table 3) and a heterogeneous version where, as previously for the idealized topography, the medium M2 is applied above a line connecting

two points outside both hills (represented by black crosses in Fig. 6). The properties of both media have been fixed so as to be in accordance with the geological model described in Figure 1. In this model, the height of the major hill is about 70m and its half width approximately 150m which corresponds to a ratio $h/l \approx 0.2$. Therefore, it can be compared to the idealized model of the previous section.

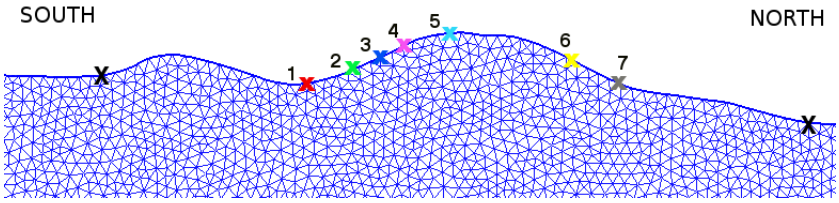

Fig. 6: South-north 2D profile of the Rognes area and locations of the 7 virtual sensors. Detail of the finite element mesh of the homogeneous model. Black crosses are the limits of the heterogeneous model.

Table 3: Characteristics of the media of the homogeneous and heterogeneous models of Rognes.

	ρ(kg/m^3)	Vp(m/s)	Vs(m/s)
M1	2100	3927	2100
M2	2000	1122	600

First, we study the amplification at the surface considering vertical SV plane waves of central frequencies 1.0, 2.0 and 5.0Hz. As previously, an amplification ratio A is calculated for the time solutions of the Vx component by respect to the incident wave. We present, in Fig. 7, these ratios at the 7 surface virtual sensors for the homogeneous (left) and heterogeneous (right) models. The geometry of the model as well as the location of the sensors have been added at the bottom of the figures for more clarity. When comparing the figures, we note a higher amplification in the heterogeneous case, with values greater than 2.5, compared to the homogeneous one, whatever the value of the frequency. More, in the homogeneous case, at fc=5.0Hz, a clear deamplification is observed outside the hill top. We note also a larger variability of the results of the heterogeneous case: the

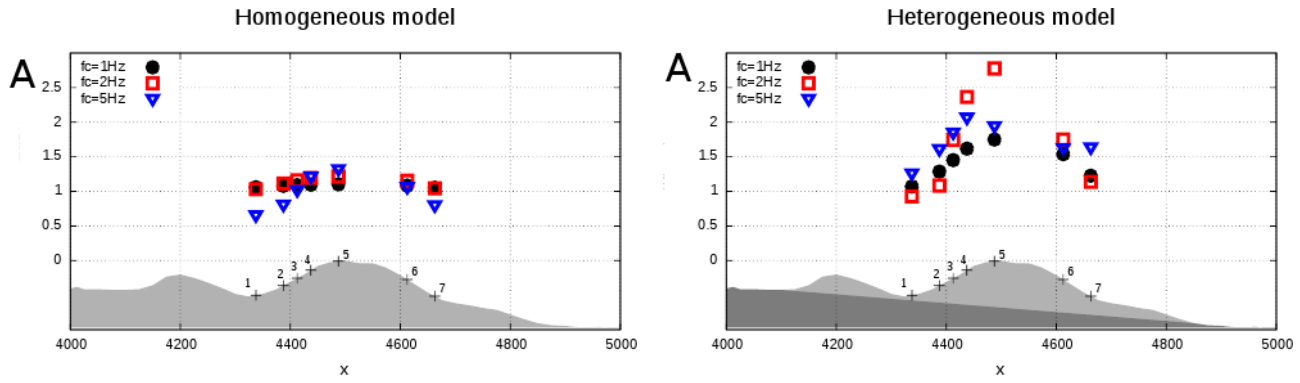

Fig. 7: Amplification ratio A of Vx at the 7 virtual surface sensors for the 2D profile of Rognes, homogeneous model (left) and heterogeneous model (right). Vertically incident plane waves of central frequency fc=1.0, 2.0 and 5.0Hz. The hill topography is included in grey at the bottom of the figures (the grey scale distinguishes the homogeneous and heterogeneous models) as well as the location of the sensors on the topography.

amplification is more dependent on the frequency of the incident wave but also on the position of the sensors on the surface. In all cases, the maximum amplification is obtained at the hill top.

In a second step, we study the influence of the angle of incidence and consider various angles $a \in \{-20, -10, -15, -50, 0, 5, 10, 15, 20\}$. As previously, we calculate amplification ratios A at the virtual sensors for the Vx component. The results are presented in Fig. 8 where the left figures correspond to the homogeneous medium and the right ones to the heterogeneous model. We have also split the results corresponding to the various values of frequency in different figures. In the homogeneous case, we notice that the amplification is very moderate except for *fc*=5.0Hz. No amplification is observed at *fc*=1.0 and 2.0Hz and the solutions do not depend on the angle of incidence. The variability of the ratios with the value of *a* increases with the value of the frequency. Finally, for *fc*=5.0Hz, amplifications higher than 1.3 are obtained at sensors 2, 3, 4 and 5 for the highest values of *a*. In the heterogeneous case (right figures), the level of amplification is higher whatever the value of the frequency with ratios greater or equal to 2.0 at the hill top. The solutions do not depend on the angle of incidence for *fc*=1.0 and 2.0Hz ; the amplification values exactly follow the surface geometry. The stronger amplification is obtained for *fc*=2.0Hz. Finally, the higher variability by respect to the angle of incidence occurs for *fc*=5.0Hz. These results can be connected to experimental and numerical studies at Tarzana hill [4,3] or in Haïti [6] describing the influence of the low velocity zone in the high amplification levels recorded in smooth topographies.

To conclude this study, we plot the transfer functions, in the case of vertical incidence, at three particular sensors (1, 3 and 5) for a comparison with the experimental data. These have been selected for their similarity with the real stations, concerning the location; Station 1 is comparable to real station EGLI, station 3 to FOUS and station 5 to FOUH, as described in Fig. 2. We present in Fig. 9, the transfer functions corresponding to the homogeneous (left) and heterogeneous (right) profiles, simulations in full lines and measurements in dashed lines. We notice that the level of amplification is very low in the homogeneous case and very different from the recordings data. On the other hand, the results of the heterogeneous model are very close to the experimental data. We observe an amplification between 4 and 7 at about 2.0Hz for the stations 3 and 5. For station 1, amplification is very low until 5.0 Hz. These results are in complete accordance with the amplification ratios of Fig. 7, presenting, in the heterogeneous case, a high amplification at *fc*=2.0Hz for virtual stations 3 and 5. In absence of data about the medium attenuation, numerical simulations have been done considering a linear elastic medium, which explains that both numerical and experimental results can be compared only at low frequency. Considering the simple 2D profile used for the simulations, these results are very encouraging and prove the need for 2D accurate models. A comparison with EC8 aggravation factors would be an interesting perspective to this work. Note however that, in the heterogeneous case, amplification values are well above the limit of 1.4 at many locations.

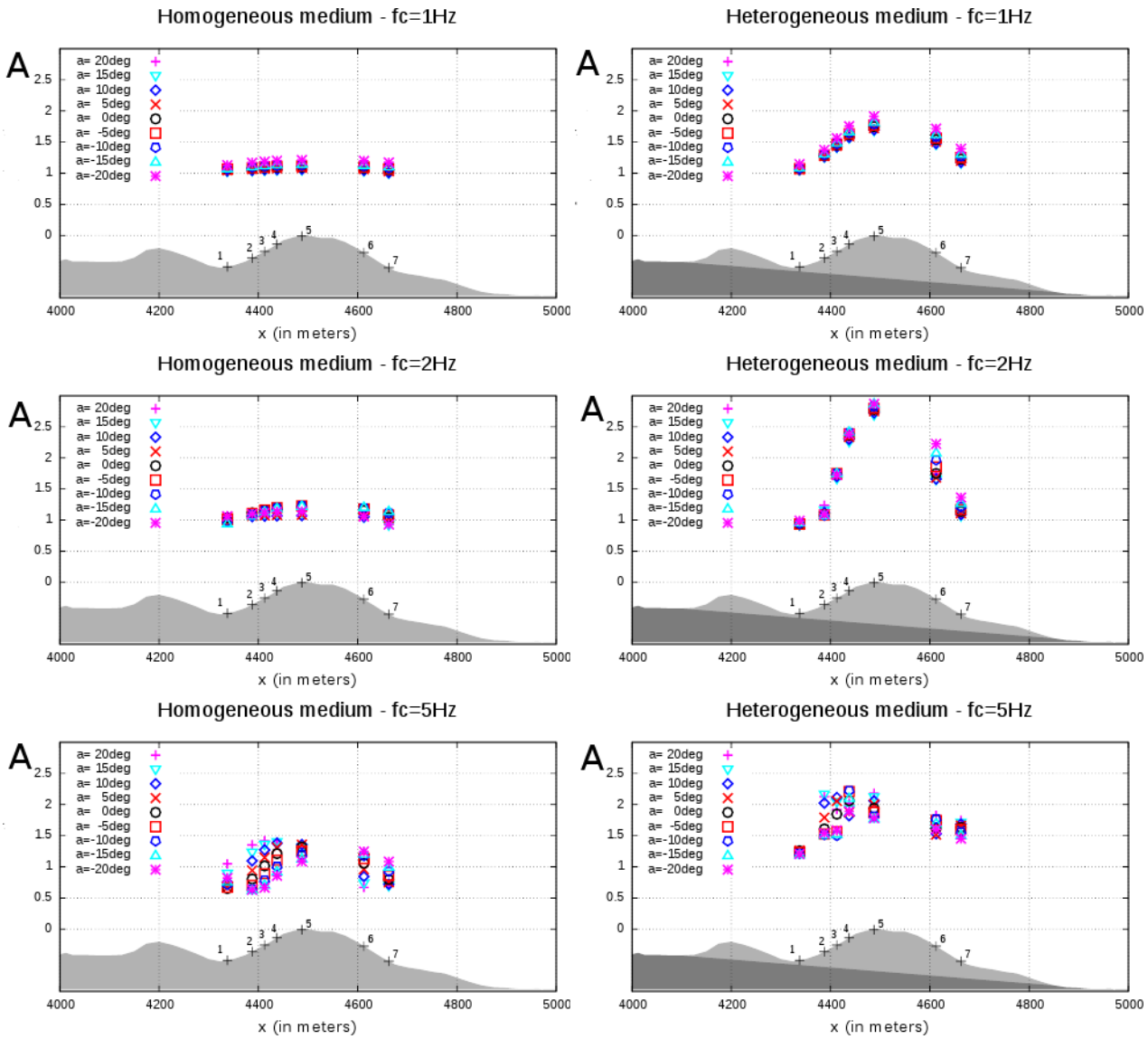

Fig. 8: Amplification ratio of Vx at the 7 virtual surface sensors for the 2D profile of Rognes, homogeneous model (left) and heterogeneous model (right). Each figure represents incident plane waves of central frequency *fc*=1.0, 2.0 and 4.0Hz. Various angles of incidence between –20deg and 20deg. The hill topography is included in grey at the bottom of the figures (the grey scale distinguishes the homogeneous and heterogeneous models) as well as the location of the sensors on the topography.+

5. Conclusion

We present a study of the topographical effects using numerical simulations by a discontinuous Galerkin finite element method. This method allows an accurate approximation of the topography via the use of unstructured triangular meshes as well as the heterogeneities in the medium. A particular treatment at the boundary allows non-vertical plane waves. The objective of this study is to reproduce the results of a field operation [5] which highlighted site effects in Rognes and explains the significant damage during the 1909 Provence earthquake. For this, two different geometries have been considered: an idealized topography and a realistic 2D profile of Rognes area. In both cases, we have studied the seismic response of the topography to series of plane shear waves. We have investigated the effects of several parameters: 1) the frequency of the incident wave, 2) its angle of incidence and 3) the in-depth medium, comparing homogeneous and heterogeneous models. In this work, we

focus on the case of gentle slopes configurations, as it is the case in Rognes; a more general parametric study including other values of shape ratios is the subject of an article in progress.

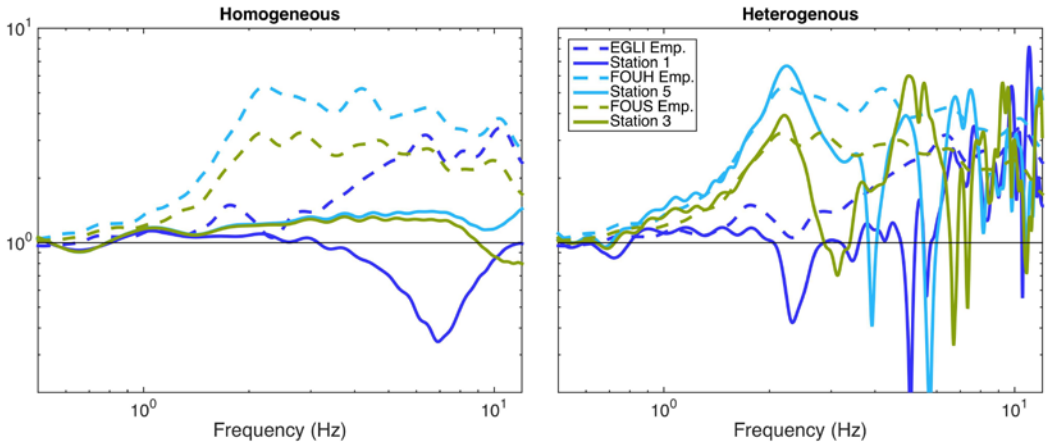

Fig. 9: Transfer functions of the Vx component for three virtual sensors for the homogeneous (left) and the heterogeneous (right) models. Spectral ratios are calculated by respect to twice the incident value.

First, for the idealized homogeneous model, we do not observe significant amplification for vertical plane waves. In the heterogeneous case, we obtain amplification ratios greater than 2 at the lowest frequencies. The use of non vertical incidence results in higher amplifications, whatever the model (homogeneous or heterogeneous). The amplification area can reach the whole topography surface.

Similar results have been obtained using the realistic profile of the Rognes area. The response of the homogeneous model to vertical plane waves is limited to low amplifications, essentially at the hill top. For the heterogeneous model, the amplification level is higher and all virtual sensors are concerned, for at least one frequency. When the angle of incidence varies, the variability increases with the frequency. For *fc*=1.0 and 2.0Hz, amplification do no depend on the angle of incidence. In the heterogeneous case, amplification reaches values up to 2.5 and a high variability is observed, especially at *fc*=5.0Hz. Finally, the transfer functions corresponding to the vertical case numerical simulations have been compared to the experimental data at three particular locations. The amplification frequencies are in good accordance when the heterogeneous model is used for simulations. Given the simplicity of the geological heterogeneous model and the hypothesis of linear elastic medium, these results are very encouraging.

This study has highlighted the influence of the medium in-depth and the angle of incidence in the amplification levels recorded at the surface of simple or gentle slopes configurations. This explains, with other parameters such as 3D effects, the differences often encountered between measurements and simulations based on homogeneous models and vertical plane waves. These results can be connected to experimental and numerical studies at Tarzana hill [4,3] or in Haïti [6] which describe the influence of the low velocity zone in the high amplification levels recorded in smooth topographies. Massa et al. [2] refer to « atypical topographic effects » when important structural and lithological heterogeneities are present. Extensions to 3D configurations and introduction of the medium attenuation constitute improvements to this work.

5. Acknowledgements

The authors thank Julie Régnier for processing the data.

6. References

[1] Singh S.K., Mena E., Castro R. (1988). Some aspects of source characteristics of the 19 september 1985 Michoacan earthquake and ground motion amplification in and near Mexico city from strong motion data. *Bull. Seism. Soc. Am.*, **78**, 451-477.

[2] Massa M., Barani S., Lovati S. (2014): Overview of topographic effects based on experimental observations: meaning, causes and possible interpretations. *Geophys. J. Int.*, **197**(3), 1551-1565.

[3] Spudich P.A., Hellwig M., Lee W.H.K. (1996).Directional topographic response at Tarzana observed in aftershocks of the 1994 Northridge, California. *Bull. Seism. Soc. Am.*, **86**(1B), S193-S208.

[4] Graizer V. (2009). Low-velocity zone and and topography as the source of site amplification effect on Tarzana hill, California. *Soil Dynamics and Earthquake Engineering*, **29**, 324-332.

[5] Duval A.-M., Bertrand E., Régnier J., Glinsky N., Langlaude P., Pernoud M., Vidal S., Gance J., Grasso E., Semblat J.-F. (2009):Experimental and numerical approaches of topographic site effects claimed to be responsible for 1909 Provence earthquake damage distribution. *AGU Fall Meeting*,, San Francisco, USA.

[6] Assimaki D., Jeong S. (2013). Observations at Hotel Montana during the M 7.0 Haïti Earthquake: Topography or Soils Amplifications? *Bull. Seism. Soc. Am.*, **103**(5), 2577-2590.

[7] Boore D.M. (1972). A note on the effect of simple topography on seismic SH waves. *Bull. Seism. Soc. Am.*, **62**(1), 275-284.

[8] Smith W.D. (1975). The application of Finite Element analysis to body wave propagation problems. *J. R. Astr. Soc.*, **42**, 747-768.

[9] Bard P.-Y. (1982). Diffracted waves and displacement field over two-dimensional elevated topographies. *Geophys. J. R. Astr. Soc.*, **71**, 731-760.

[10] Bouckovalas G.D. and Papadimitriou A.G. (2005). Numerical evaluation of slope topography effects on seismic ground motion, *Soil Dynamics and Earthquake Engineering*, **25**, 547-558.

[11] Bouchon M., Schultz C.A., Toksoz M.N. (2010). Seismic response of a hill: the example of Tarzana, California. *Bull. Seism. Soc. Am.*, **86**(1A), 66-72.

[12] Bard P.-Y., Tucker B.E. (1985). Underground and ridge site effects: a comparison of observation and theory. *Bull. Seism. Soc. Am.*, **75**(4), 905-922.

[13] Géli L., Bars P.-Y., Jullien B. (1988). The effect of topography on earthquake ground motion: A review and new results. *Bull. Seism. Soc. Am.*, **78**(1), 42-63.

[14] Chardon D., Bellier O. (2003): Geological boundary conditions of the 1909 Lambesc (Provence, France) earthquake: structure and evolution of the Trévaresse ridge anticline. *Bull. Soc. Géol. Fr.*, **174** (5), 497-510.

[15] Glinsky N., Bertrand E. (2012). Topographical site amplifications investigations by combining numerical and field experiments : the case of Rognes, south east France. *15 WCEE Conference*, Lisboa (Portugal).

[16] Delcourte S., Fezoui L., Glinsky N. (2009). A high-order discontinuous Galerkin method for the seismic wave propagation. ESAIM: Proc., 27, 70-89.

[17] Delcourte S., Glinsky N. (2015). Analysis of a high-order space and time discontinuous Galerkin method for elastodynamic equations. Application to 3D wave propagation. *ESAIM: Math. Model. And Numer. Anal,*. **49**, 1085-1126.

[18] Gaffet S., Bouchon M. (1989). Effects of two-dimensional topographies using the discrete wavenumber boundary integral equation method in P-SV cases. *J. Acous. Soc. Am.*, **85**,2277-2283.

[19] Geuzaine C., Remacle J.-F. (2009). Gmsh a three-dimensional finite element mesh generator with built-in pre- and post-processing facilities. *Int. J. Numer. Meth. Engng.*, **79**(11), 1309-1331.